

Magnon gap excitations and spin-entangled optical transition in van der Waals antiferromagnet NiPS₃

Dipankar Jana,^{1,*} P. Kapuscinski,¹ I. Mohelsky,¹ D. Vaclavkova,¹
I. Breslavetz,¹ M. Orlita,^{1,2} C. Faugeras,¹ and M. Potemski^{1,3,†}

¹*Laboratoire National des Champs Magnétiques Intenses, LNCMI-EMFL,
CNRS UPR3228, Univ. Grenoble Alpes, Univ. Toulouse,
Univ. Toulouse 3, INSA-T, Grenoble and Toulouse, France*

²*Institute of Physics, Charles University, Ke Karlovu 5, Prague, 121 16, Czech Republic*

³*CENTERA Labs, Institute of High Pressure Physics, PAS, 01 - 142 Warsaw, Poland*

Optical magneto-spectroscopy methods (Raman scattering, far-infrared transmission, and photoluminescence) have been applied to investigate the properties of the NiPS₃ semiconducting antiferromagnet. The fundamental magnon gap excitation in this van der Waals material has been found to be split into two components, in support of the biaxial character of the NiPS₃ antiferromagnet. Photoluminescence measurements in the near-infrared spectral range show that the intriguing 1.475 eV-excitation unique to the NiPS₃ antiferromagnetic phase splits upon the application of the in-plane magnetic field. The observed splitting patterns are correlated with properties of magnon excitations and reproduced with the simple model proposed. Possible routes towards a firm identification of the spin-entangled 1.475 eV-optical excitation in NiPS₃, which can hardly be recognized as a coherent Zhang-Rice exciton, are discussed.

I. INTRODUCTION

Scientific curiosity and the possible design of novel devices continue to drive pertinent research efforts focused on two-dimensional materials [1, 2]. Among systems of intense current interest are layered magnets [3, 4] and, in particular, the antiferromagnets from a large family of transition metal phosphorus trichalcogenides (TMPTC), such as MnPS₃, FePS₃, NiPS₃, CoPS₃, MnPSe₃, and many others [5–14]. The TMPTC layers are weakly coupled by van der Waals forces. The magnetic ordering in these antiferromagnets is largely governed by the spin-spin exchange interactions within the layers whereas the interlayer exchange integrals are rather small [12, 15]. This justifies the two-dimensional character of such magnetic systems even in their bulk form. The magnetic anisotropies (of single ions or due to dipolar spin interaction) is another key element that affects the magnetic properties of TMPTC antiferromagnets, establishing the direction of spin ordering and character of magnon excitations (magnon gaps in particular) [16, 17]. Two groups of TMPTC antiferromagnets can be distinguished: the group of nearly uniaxial antiferromagnets such as, for example, MnPS₃ and FePS₃ with spins oriented mostly perpendicular to the layer plane [6–9, 18] and another group of TMPTC antiferromagnets with spins oriented in the layer planes, which generally represent the biaxial systems (with non-negligible magnetic anisotropy fields along two different axes) [12, 14, 19, 20]. Whereas numerous works have been devoted to reveal the properties of the former-group antiferromagnets, the in-plane TMPTC antiferromagnets are less understood.

Particularly controversial are the properties of NiPS₃, both with respect to its characteristic magnon excitations [12, 19, 21–23] as well as in regards to the intriguing optical transition in the near-infrared spectral range, which is observed in this material only below Néel temperature, $T_N \approx 155$ K [11, 24, 25]. Bulk NiPS₃ in its antiferromagnetic state, in which spins are aligned in the layers' planes, has been initially considered to be uniaxial, with a characteristic double degenerated fundamental magnon gap [19]. On the other hand, lifting of the magnon gap degeneracy into two components has been evoked in more recent reports, thus pointing out towards the biaxial character of the NiPS₃ antiferromagnet [12, 21]. Nevertheless, the identification of these two magnon-gap components is not fully transparent, including a noticeable spread of the reported energy values [12, 19, 21–23] and of the associated amplitude of the spin-flop field [25–28]. Perhaps even more confusing is the understanding of a sharp and strongly linearly polarized optical transition, which appears in NiPS₃ at ≈ 1.475 eV only in the antiferromagnetic phase [11, 24, 25]. Appealingly enough, this transition has been identified as a collective excitation, the spin-entangled excitonic transition between Zhang-Rice triplet and singlet states [11]. In support of such an assignment, this exciton has been claimed to be robust to the application of a magnetic field [11]. On the other hand, the axis of its linear polarization has been more recently shown to follow the direction of the Ni²⁺ spins' alignment, which, notably can rotate with the applied in-plane magnetic field [25].

In this paper, the biaxial character of the NiPS₃ antiferromagnet is confirmed via the observation of two low-energy excitations, at 1.25 ± 0.13 meV (10 ± 1 cm⁻¹) and 5.33 ± 0.06 meV (42.5 ± 0.5 cm⁻¹) as measured at low temperature, which we identify as two components of the fundamental magnon gap in this antiferromagnet. These excitations soften with temperature and show the evolu-

* dipankar.jana@lncmi.cnrs.fr

† marek.potemski@lncmi.cnrs.fr

tion with the applied magnetic field as expected for a biaxial antiferromagnet. The analysis of the data provides a set of parameters (such as the ratio of the anisotropy fields, the spin-flop field, and the effective g -factor) that characterize the antiferromagnetic phase of NiPS₃.

On the other hand, our examination of the optical response of NiPS₃ in the near-infrared spectral range sheds new light on the properties of the attention-catching optical excitation (at ≈ 1.475 eV) in this antiferromagnet. In striking contrast to recent claims [24], we observe that this transition shows a prominent splitting when the field is applied along the plane directions. The amplitude of this splitting depends on the direction of the applied magnetic field with respect to the spin orientation and it substantially collapses above the spin-flop field. The properties of this 1.475 eV-excitation are correlated with those of magnon-gap excitations and we propose a simple formalism to ascribe the observed splitting pattern.

II. EXPERIMENTAL DETAILS

The applied experimental techniques include a variety of optical spectroscopy methods: micro Raman scattering, far-infrared absorption, as well as micro-photoluminescence spectroscopy in the near-infrared spectral range. When needed and feasible, the optical response has been measured as a function of temperature, as a function of the external magnetic field, in different configurations of the direction of the magnetic field with respect to the spin alignment, and also employing polarization resolved techniques.

The samples used in our experiments were extracted from commercially available NiPS₃ crystals. Large area (≈ 1 cm²) and rather thick (≈ 1 mm) species were used for far-infrared magneto-absorption measurements. Instead, smaller size specimens (≈ 1000 $\mu\text{m}^2 \times 5$ μm) were prepared for Raman scattering and optical measurements in the near-infrared range. Those samples consisted of rather homogeneous flakes which were mechanically exfoliated from bulk crystals and deposited on a silicon substrate with the help of the dry-transfer technique. More experimental details can be found in the Supplemental Material (SM) [29].

III. EXPERIMENTAL RESULTS AND DISCUSSION

The magnetic structure of the NiPS₃ antiferromagnet, as it emerges from recently reported studies, [12] is shown in Fig. 1. The collinear nickel magnetic moments are aligned in the layers' a - b planes, along the a -axis. Such arrangement of Ni²⁺ spins is assumed to be imposed by the anisotropy field along the c -axis (which forces the spin alignment in the layer plane) and another, likely weaker, anisotropy field along b -axis which aligns spins along the a -axis. The net antiferromagnetic spin

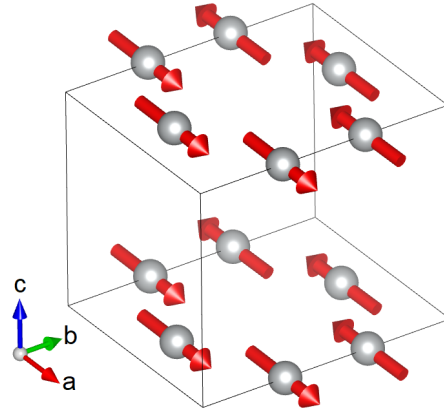


FIG. 1. The magnetic structure of NiPS₃ in its antiferromagnetic phase. Grey spheres and red arrows represent Ni²⁺ ions and spin direction, respectively. The figure is created using the VESTA software package [30].

order is believed to be due to the strong, third-neighbor antiferromagnetic-type exchange coupling between Ni²⁺ spins in the plane. The weaker, nearest-neighbor in-plane and between-the-planes exchange interactions are ferromagnetic. The second neighbor exchange interaction seems to be even weaker.

A. Low-energy spin wave excitations

The presence of two anisotropy fields, i.e., the biaxial character of the NiPS₃ antiferromagnet, imposes the splitting of its fundamental magnon gap into two components. As shown below, these two low-energy spin-wave excitations (magnons) at the $k = 0$ point of the Brillouin zone, can be traced with Raman scattering experiments, and the upper energy mode is also visualized with far-infrared transmission measurements. While the Raman scattering technique has been already applied to study NiPS₃ specimens, only the strong response due to the characteristic phonon modes that appear at relatively high energies have been investigated so far [13, 24, 25]. Instead, in our experiments we concentrate on the Raman scattering response in the close vicinity, ± 50 cm⁻¹, of the laser line. As shown in Fig. 2, two distinct excitations are observed in this spectral range. They are labeled as M_+ and M_- in the Stokes Raman scattering signal and have their M'_+ and M'_- counterparts in the anti-Stokes spectra. It is worth noticing that Raman scattering features related to our low-energy modes are significantly less intense than those due to phonons observed at higher energies (see Fig. S1 of SM) [29]. From the data illustrated in Fig. 2 we read that in the limit of low temperatures the characteristic energies of our $M_{+/-}$ excitations are, respectively, $w_{M_+} \cong 43$ cm⁻¹ and $w_{M_-} \cong 10$ cm⁻¹.

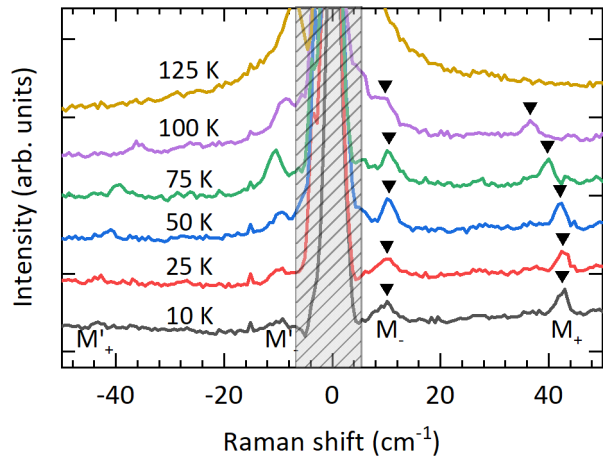


FIG. 2. Raman scattering spectra of NiPS₃ antiferromagnet measured at selected temperatures. M₊ (M₊') and M₋ (M₋') resonances correspond to Stokes (anti-Stokes) modes of the split components of magnon gap excitation. Spectra are shifted vertically for clarity. Peak energies of Stokes modes are marked by black triangles. The shaded region marks the spectral range blocked by the Bragg filters.

These energies decrease when the temperature is raised; the effect being particularly well visible for the case of the upper energy M₊ mode. When approaching the Néel temperature the M₊ significantly broadens and the M₋ mode merges into the enlarged laser tail. The observed, temperature-activated softening of M_{+/−} modes stands for the primary indication that they are associated with the magnon gap excitations.

To further elucidate the origin of our M_{+/−} modes as two low-energy magnon gap excitations, we examine their evolution upon the applied magnetic field, as investigated at low, $T = 4.2$ K, temperature. First, we consider the configuration of the magnetic field applied in the direction along the layer plane. The data obtained for three different NiPS₃ flakes are presented in Fig. 3. As can be seen in this figure, there is a perceivable evolution of the M_{+/−} modes with the applied magnetic field, albeit it is clearly different for each set of the data. It is logical to expect that the magnetic field evolution of the M_{+/−} modes might be critically altered by the actual experimental geometry, mainly the magnetic field direction with respect to the direction of the spin alignment (at $B = 0$ T), i.e., with respect to the a -axis of the NiPS₃ crystal. Although the orientation of the a, b crystal axes with respect to the direction of the applied magnetic field has not been independently determined in our work, we found it to be different in the three flakes investigated.

To interpret the observed dependencies of M_{+/−} energies on the strength of the applied in-plane magnetic field ($B = \mu_0 H$) we refer to the mean-field theory of antiferromagnetism [31], according to which the $w_{+/−}(B)$ dependencies of the magnon gap energies in a

simple biaxial antiferromagnet are given by two (positive) solutions of the following, $F(w) = 0$, equation:

$$\begin{aligned}
 F(w) = & \left(\frac{w}{g\mu_B} \right)^4 - \left(\frac{w}{g\mu_B} \right)^2 [B^2 (\cos^2 \Psi + 1) + C_2 \\
 & + C_1 \{ \cos^2 (\Psi - \theta_B) - 2 \sin^2 (\Psi - \theta_B) \}] + B^4 \cos^2 \Psi \\
 & - B^2 [C_1 \{ \cos^2 \Psi \cos 2(\Psi - \theta_B) \\
 & + \cos \Psi \sin \theta_B \sin (\Psi - \theta_B) + \sin \Psi \cos \theta_B \sin (\Psi - \theta_B) \} \\
 & + C_2 (\cos^2 \Psi - \sin^2 \Psi)] \\
 & + C_1 \cos 2(\Psi - \theta_B) \times [C_2 - C_1 \sin^2 (\Psi - \theta_B)] = 0
 \end{aligned} \tag{1}$$

where g is the effective g -factor and μ_B stands for the Bohr magneton. θ_B is the angle between the direction of the applied magnetic field and the initial (at $B = 0$ T) spin alignment direction (along a -axis). The constants C_1 and C_2 are given by

$$C_1 = 2B_J B_{D-b}, \quad C_2 = 2B_J B_{D-c} \tag{2}$$

Here, B_J , B_{D-b} and B_{D-c} are, respectively, the effective exchange field, and the anisotropy fields along the easy b - and hard c -axis. As illustrated in Fig. S2 of SM, [29] when $\theta_B \neq 0$, the application of the external magnetic field progressively rotates the magnetic moments towards the direction perpendicular to the field, while the moment directions of two spin sublattices keep being opposite in a wide range of the magnetic field, due to strong exchange coupling. Canting of spins, towards their unavoidable ferromagnetic alignment (along the magnetic field) is likely apparent in the range of very high magnetic field, hardly available in our experiments.

The apparent rotation, Ψ , of the spins' alignment with respect to the magnetic field direction is given by the following equation [31]:

$$\tan 2\Psi = \frac{\sin 2\theta_B}{\cos 2\theta_B - B^2/B_{sf}^2} \tag{3}$$

where, B_{sf} is the spin-flop field. When setting $B = 0$ ($\Psi = \theta_B$), the two roots of Eq. 1 are:

$$\begin{aligned}
 w_{M-}(B=0) &= g\mu_B \sqrt{C_1} = g\mu_B \sqrt{2B_J B_{D-b}} \\
 w_{M+}(B=0) &= g\mu_B \sqrt{C_2} = g\mu_B \sqrt{2B_J B_{D-c}}
 \end{aligned}$$

which account for the energies of two non-degenerate low-energy magnon modes that appear in a biaxial antiferromagnet in the absence of the magnetic field.

The two, $w_{M+}(B)$ and $w_{M-}(B)$ solutions of Eq. 1 for several, different values of θ_B are illustrated in Fig. S3 of SM [29]. Notably, if $\theta_B = 0$ then in the range of $B < B_{sf}$:

$$\begin{aligned}
 w_{M+} &= g\mu_B \sqrt{C_2 + 3B^2} \\
 w_{M-} &= g\mu_B \sqrt{C_1 - B^2}
 \end{aligned}$$

and we note that $w_{M-}(B)$ reaches its zero value at the spin-flop field $B_{sf} = \sqrt{C_1}$. In this particular case, the arrangement of the Ni²⁺ magnetic moments is such that they remain aligned along the a -axis until B_{sf} is

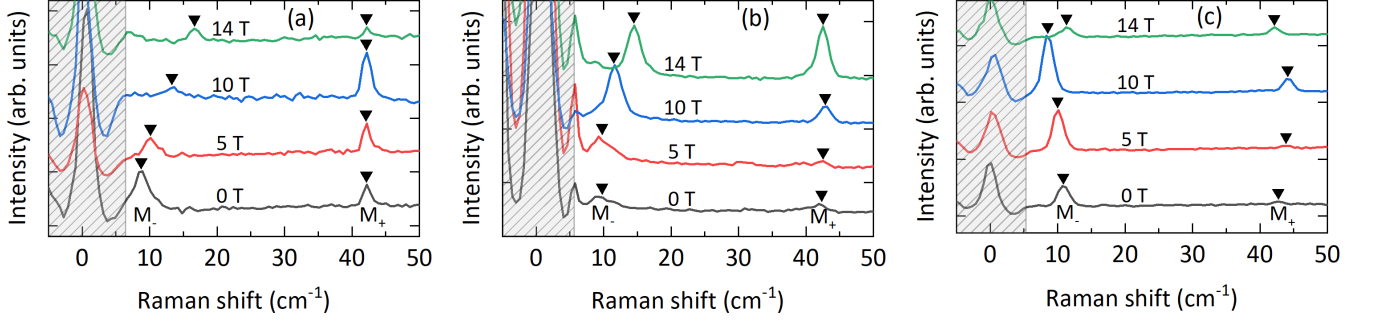


FIG. 3. (a), (b) and (c) Low temperature (4.2 K) Raman scattering spectra of exfoliated NiPS_3 flakes in three different orientations of the crystal a -axis (i.e. with respect to spin alignment at $B = 0$) with respect to the in-plane magnetic field. Magnon gap excitations (M_+ and M_-) are marked by a black triangle. Spectra are shifted vertically for clarity. The shaded region marks the spectral range blocked by the Bragg filters.

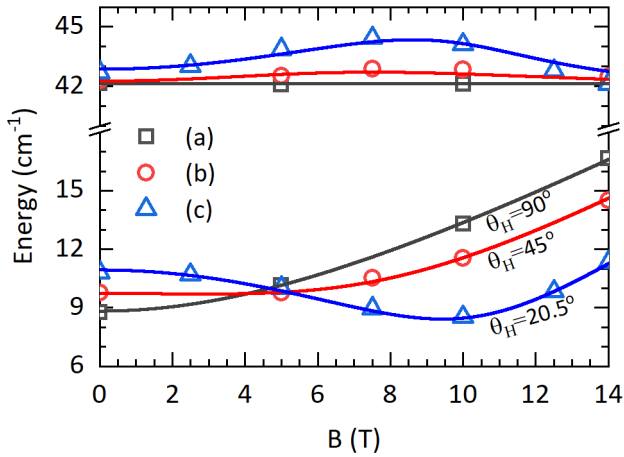


FIG. 4. In-plane magnetic field dependence of M_+ and M_- magnon excitation energies at 4.5 K as extracted from the results of Raman scattering measurements, illustrated in Fig. 3. The simulated field dependence for $\theta_B = 90^\circ, 45^\circ$ and 20.5° are also shown by solid lines on the same graph. The same g -factor ($g = 2.15$) has been considered for three flakes.

reached, at which spins flop abruptly to be aligned in the direction perpendicular to the external field, (i.e. along b -axis) though conserving the antiferromagnetic order.

The energies of M_+ and M_- excitations, extracted from the results of magneto-Raman scattering measurements, illustrated in Fig. 3, for three different NiPS_3 flakes, are shown in Fig. 4. The three pairs of $w_{M_+}(B)$ and $w_{M_-}(B)$ dependencies are clearly different what points out different experimental geometries (different θ_B angle) for each of three data sets. Solid lines in Fig. 4 represent the fitted dependencies according to Eq. 1. The simulation of each pair of $w_{M_+}(B)$ and $w_{M_-}(B)$ dependencies implies the use of four fitting parameters: g (the effective g -factor), C_1 (or the related energy $w_{M_-} = g\mu_B\sqrt{C_1}$), C_2 (or $w_{M_+} = g\mu_B\sqrt{C_2}$) and the angle θ_B . As expected the three

extracted values of $\theta_B = 90^\circ, 45^\circ$ and 20.5° are significantly different. The g -factor, $g = 2.15$ has been found to be common for three flakes. The magnon energies at zero magnetic field are somewhat scattered: $(w_{M_-}, w_{M_+}) = (9 \text{ cm}^{-1}, 42 \text{ cm}^{-1})$, $(10 \text{ cm}^{-1}, 42 \text{ cm}^{-1})$ and $(11 \text{ cm}^{-1}, 42.8 \text{ cm}^{-1})$, respectively for (a), (b) and (c) data sets (see Fig. 4). Slightly different magnon energies for our three flakes may be due to their different thickness and/or the induced strain [19]. Setting $w_{M_-} = 10 \text{ cm}^{-1}$ and $w_{M_+} = 42.5 \text{ cm}^{-1}$ we derive $B_{sf} = w_{M_-}/g\mu_B = 10.4 \text{ T}$ for the spin-flop field and $B_{D-c}/B_{D-b} = (w_{M_+}/w_{M_-})^2 = 18$ for the ratio of the hard- to easy-axis anisotropy fields.

Turning now the attention to the configuration of the magnetic field applied perpendicularly to the layers' planes ($B \parallel c$) we note that in this case all spins, independent of their in-plane orientation, are aligned perpendicularly to the direction of the B -field. When $B \parallel c$, the magnon gap energies versus the magnetic field are given by simple formulas [31]:

$$w_{M_-} = g\mu_B\sqrt{C_1} \quad w_{M_+} = g\mu_B\sqrt{C_2 + B^2} \quad (4)$$

The M_- mode is not affected by the magnetic field whereas w_{M_+} increases monotonically with B .

When setting the $B \parallel c$ configuration, the performance of our magneto-Raman scattering set-up appeared to be not sufficient enough for measurements of low-energy excitations. The encountered problems to efficiently reduce the stray laser light could be, however, overcome when tilting the sample, i.e., when setting a certain angle $\angle(B, c)$ between the direction of the magnetic field and the crystal c -axis. The magneto-Raman scattering spectra measured in the tilted, $\angle(B, c) = 20^\circ$ configuration are illustrated in Fig. 5. In such a configuration the dispersion of M_- and M_+ modes with the magnetic field cannot be expected to exactly follow the predictions otherwise valid for the ideal case of $B \parallel c$ geometry. Nevertheless, the overall trends are in agreement with Eq. 4: w_{M_+} increases monotonically with B whereas the M_- mode is unaffected by the magnetic field.

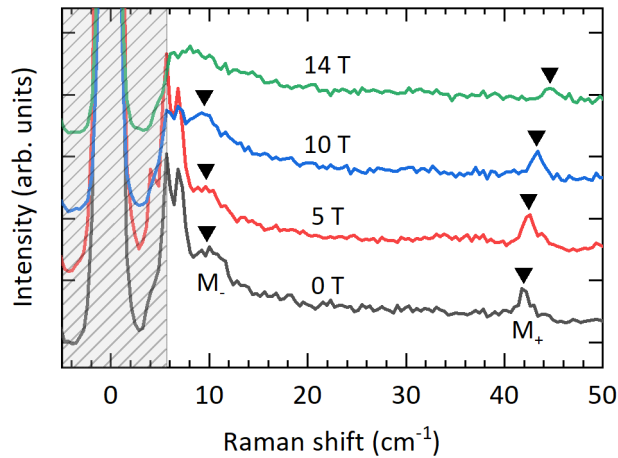


FIG. 5. Low temperature (4.2 K) Raman scattering spectra of exfoliated NiPS₃ flake at selected strength of the magnetic field applied in the direction tilted by 20° with respect to the crystal c-axis. The spectra are shifted vertically for clarity. Peak energies of magnon excitation modes are marked by the black triangle. The shaded region marks the spectral range blocked by the Bragg filters.

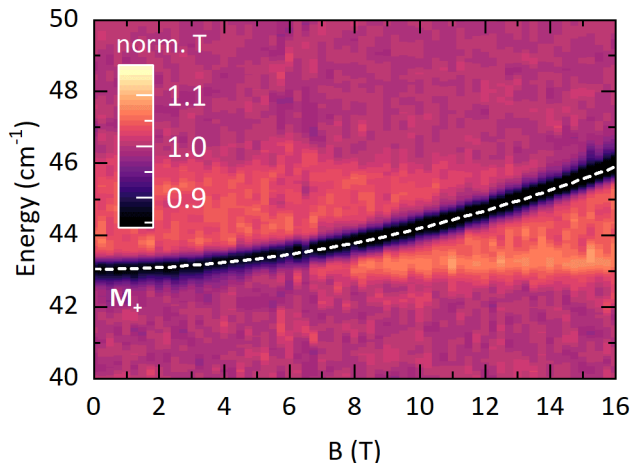


FIG. 6. False color map of normalized far-infrared transmission of NiPS₃, measured at 4.2 K, as a function of the magnetic field applied along the crystal c-axis. Dashed line corresponds to fit a of the $w_{M_+}(B)$ dependence according to Eq. 4.

Another possible method to trace the magnon gap excitations in antiferromagnets is a direct measurement of light absorption/transmission associated with these modes in the far infrared (FIR) spectral range [8]. The advantage of this technique, in conjunction with the application of the magnetic field, is that it can be easily set in the $B \parallel c$ configuration (Faraday geometry). We must, however, admit that our large NiPS₃ specimens, which are imperative for FIR transmission experiments, are composed of differently oriented, in the $(a-b)$ -plane,

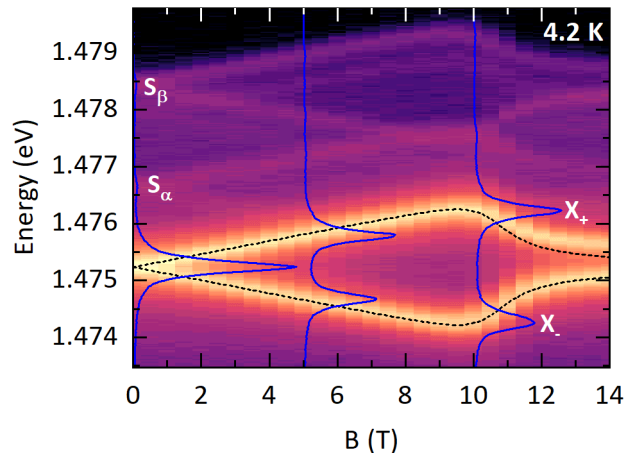


FIG. 7. False color map of low temperature (4.2 K) PL of NiPS₃ exfoliated flake as a function of the in-plane magnetic field. Few representative PL spectra, measured at a magnetic field strength of 0 T, 5 T, and 10 T, are also plotted. Dashed lines correspond to a fit of the $E_{X_{+/-}}$ dependence according to Eq. 5 for $g = 2.0$, $B_{sf} = 10.55$ T and $\theta_B = 5^\circ$. High energy satellite peaks are labeled as S_α and S_β .

crystal grains. This fact does not affect the analysis of the magneto-spectroscopy data in the $B \parallel c$ geometry (all Ni²⁺ spins are aligned perpendicularly to B), but makes FIR magneto-spectroscopy hardly applicable in the configuration of B applied in the $(a-b)$ -plane (magnon mode dispersion with B depends critically on actual, B versus a -axis orientation). The results of FIR magneto-transmission measurements carried out at low temperature (4.2 K) in the Faraday geometry on bulk NiPS₃ samples are illustrated in Fig. 6. A clear absorption feature observed in these data, along with its characteristic evolution with the magnetic field, is identified as due to the M_+ excitation. Unfortunately, the detection of the low-energy M_- mode was beyond the limit of our experimental setup. Using the adequate, for $B \parallel c$ geometry, formula (see Eq. 4), the $w_{M_+}(B)$ dependence is simulated (dashed line in Fig. 6) when setting $w_{M_+} = 43$ cm⁻¹ and $g = 2.15$, the latter value is in perfect agreement with the estimation of this parameter from magneto-Raman scattering experiments.

B. Spin entangled optical excitation

The optical absorption edge in NiPS₃ is located at ~ 1.8 eV but this crystal is also known to exhibit several optical transitions below its optical bandgap [24]. Particularly intriguing are the properties of an exceptionally sharp transition which gives rise to both the photoluminescence (PL) and absorption-type signal at an energy of ≈ 1.475 eV. As already reported [25] and confirmed in our study (see Fig. S4 of SM) [29], this transition,

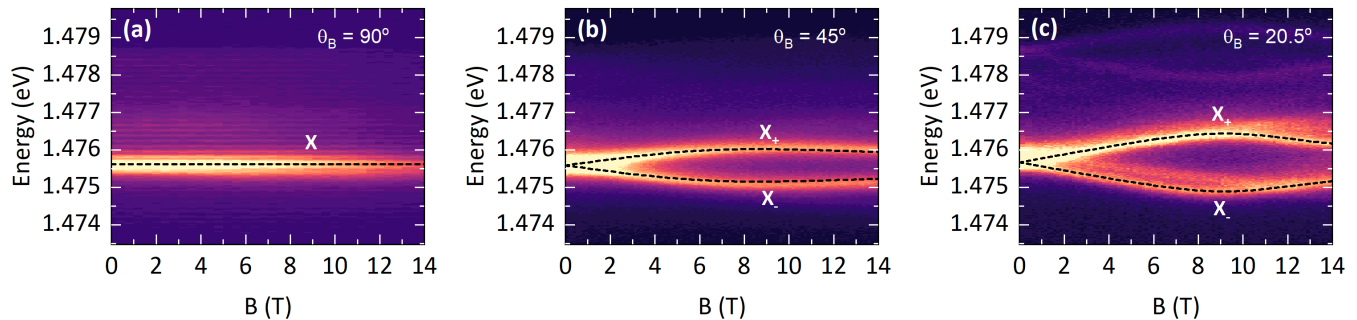


FIG. 8. (a), (b) and (c) False color map of low temperature (4.2 K) PL of NiPS₃ exfoliated flakes as a function of the in-plane magnetic field with identical spin orientations as in Fig. 3. Dashed lines correspond to a fit of the $E_{X_{+/-}}$ dependence according to Eq. 5 for $g = 2.0$.

referred to here as X-transition, is sensitive to spin ordering: it appears only in the antiferromagnetic phase and displays a high degree of linear polarization, the axis of which follows the direction of spin alignment. The X-transition has been previously identified as a many-body-in-nature bosonic excitation/exciton involving the Zhang-Rice triplet and singlet states [11]. In support of this concept, the X-transition has been reported to be robust with respect to the applied magnetic field. That is, however, in contradiction with the results of the present experiments.

A remarkable evolution of the X-transition under the applied field is illustrated in Fig. 7 with a representative collection of the PL spectra measured, at low temperature (4.2 K), as a function of the in-plane magnetic field. In the absence of the magnetic field our spectra perfectly match those reported previously: a sharp (≤ 0.2 meV halfwidth) PL peak due to X-transition is observed slightly above 1.475 eV and it is followed by two/three much weaker satellites on its high energy side. Yet, the application of the in-plane magnetic field induces a splitting of the X-transition (as well as of its high energy satellites) into two, X_+ and X_- , components (see Fig. 7). The separation ΔE between the X_+ and X_- , components first increases linearly with the magnetic field but abruptly decreases when $B \geq 10$ T, i.e., above the spin-flop field. The splitting pattern of the X-transition such as that shown in Fig. 7 is, however, not the same for all investigated NiPS₃ flakes. We speculate that the actual orientation of the magnetic field with respect to the direction of the spin alignment decides about the character of the X-transition splitting. To check this hypothesis, the reported above magneto-Raman scattering measurements on three different flakes (with different B versus a -axis orientations) have been in parallel completed by magneto-PL measurements of the X-transition. The data presented in Fig. 3 (a), (b), (c) and the results presented in Fig. 8 (a), (b), (c) are, respectively, obtained for the same NiPS₃ flakes. As shown in Fig. 8 (a), the splitting of the X-transition is practically absent in the configuration when the magnetic field is applied perpendicularly to

the direction of the Ni²⁺ spins' alignment ($\theta_B = 90^\circ$ and thus $\Psi(B) = 90^\circ$, see Fig. S3a of SM [29]) but progressively appears when θ_B becomes smaller (see Fig. 8 (b), and (c)). The observed nonlinearities in the X-transition splitting must be due to the field-induced rotation of the axis of Ni²⁺ spin alignment (see Fig. S3 (a) of SM [29]). The splitting of the X-transition is therefore expected to reflect the field-induced disequilibrium of magnetic moments of Ni²⁺ spin sublattices, one of the moments being enhanced and another suppressed along the direction of the applied magnetic field. In other words, we propose that the observed splitting of the X-transition can be accounted for by the simple following formula:

$$E_{X_{+/-}} = E_{X_0} \pm g\mu_B B \cos(\Psi) \quad (5)$$

where $\Psi = \Psi(B)$ is the previously defined angle (Eq. 3) between the axis of the Ni²⁺ spins' alignment and B -direction; g stands for the effective g -factor and E_{X_0} is the energy of the X-transition at zero magnetic field. As shown with dashed lines, in Fig. 7 and Fig. 8 (a), (b) and (c), the above formula reproduces well the observed splitting patterns of the X-transition. The results were simulated assuming $g = 2.0$ for all data sets. The E_{X_0} energy has been found to scatter a bit from 1.4752 to 1.4755, depending on the flake investigated. When simulating the $E_{X_{+/-}}(B)$ dependencies for the data shown in Fig. 8 (a), (b) and (c) we have, respectively, set $\theta_B = 90^\circ, 45^\circ$ and 20.5° , as previously derived from the analysis of magnon gap excitations. As for results presented in Fig. 7 (which were not completed by Raman scattering measurements) the dashed lines follow the formula with the best-fit parameters $\theta_B = 5^\circ$ and spin flop field $B_{sf} = 10.55$ T. It is important to note that our measurements confirm a strong linear polarization of the PL spectra related to X-transition. Moreover, we observe that the polarization properties are the same for both X_+ and X_- components and the polarization axis rotates with the applied, in-plane magnetic field. The results of polarization measurements of spectra illustrated in Fig. 7 are displayed in Fig. S4 of the SI. In this case, the field-induced gradual rotation of the polarization axis is rather weak until

reaching the spin-flop field ($B_{sf} \sim 10$ T) where it shows an abrupt change. This behavior is similar to the field dependence of Ψ (see Fig. S2 and S3a of the SM) [29], which reveals a correlation of the polarization axis of the X-transition with the direction of spin alignment.

We do believe that our study reveals the overlooked but relevant properties of the X-transition in NiPS₃, which recently attracted considerable attention. The firm identification of this intriguing excitation calls for thorough theoretical analysis and is beyond the scope of our experimental work. We should, however, admit that the reported here sensitivity of the X-transition to the applied magnetic field (splitting of the transition, in particular) is in clear disagreement with the statement on the robustness of this transition to the magnetic field; the statement being an argument to assign the X-transition as due to a coherent exciton involving the Zhang-Rice triplet and singlet states [11]. An optional possibility to be considered is that our X-transition is due to an internal excitation within the $d-d$ states of Ni²⁺ ions [32]. Such, a more trivial origin of our X-transition would classify it along with a similar excitation reported for another layered semiconducting antiferromagnet, MnPS₃ [33]. The optical transition reported for MnPS₃ at ~ 2.64 eV is also pretty narrow ($\simeq 0.8$ meV half-width) and appears below the bandgap of this material, though it is identified as an internal transition within the Mn²⁺ ions. Notably, it is active only in the antiferromagnetic phase and displays the magnetic field-induced splitting, suppressed, *notabene* above the spin-flop field, thus largely resembling the properties of the X-transition in NiPS₃. The questions, however, arise why the internal transitions within the magnetic ions would be so sharp and, more importantly, why would they appear only in the antiferromagnetic phases (perhaps due to possible change in the crystal field symmetry).

IV. CONCLUSIONS

Concluding we have employed Raman scattering, far-infrared transmission, and photoluminescence spec-

troscopy measurements, carried as a function of temperature and of the magnetic field, to clarify the controversies regarding the properties of NiPS₃ van der Waals antiferromagnet. The observation of the fundamental magnon-gap excitation splitting into two components supports the identification of NiPS₃ as a biaxial antiferromagnet which we characterized with the relevant parameters (fundamental magnon-gap energies, g -factor, spin-flop field, combination of exchange/anisotropy fields). The overlooked properties of the intriguing optical transition that appear in the near-infrared spectral range have been reported. Our observations, of the magnetic field-induced splitting of this transition in particular, rise pertinent questions about its attribution as a many-body coherent excitonic transition. The reported experimental results call for thorough theoretical works, that can eventually clarify the origin of the intriguing below-band optical transition in NiPS₃. We speculate that similar "excitonic" transitions might be characteristic of other semiconducting antiferromagnets such as, for example, MnPS₃.

V. ACKNOWLEDGEMENTS

Numerous valuable discussions with A. Wildes are acknowledged. The work has been supported by the EC Graphene Flagship project. M.P acknowledges support from the Foundation for Polish Science (MAB/2018/9 Grant within the IRA Program financed by EU within SG OP Program).

D.J. performed the data analysis, wrote the preliminary version of the manuscript, and conducted the experiments together with P.K., I.M., D.V., and I.B., whereas M.O., C.F., and M.P. conceptualized the work. All authors discussed the results and contributed to setting the final version of the manuscript.

-
- [1] A. Geim and I. Grigorieva, Van der Waals heterostructures, *Nature* **499**, 419 (2013).
 - [2] G. R. Bhimanapati, Z. Lin, V. Meunier, Y. Jung, J. Cha, S. Das, D. Xiao, Y. Son, M. S. Strano, V. R. Cooper, *et al.*, Recent advances in two-dimensional materials beyond graphene, *ACS nano* **9**, 11509 (2015).
 - [3] Q. H. Wang, A. Bedoya-Pinto, M. Blei, A. H. Dismukes, A. Hamo, S. Jenkins, M. Koperski, Y. Liu, Q.-C. Sun, E. J. Telford, *et al.*, The magnetic genome of two-dimensional van der Waals materials, *ACS nano* **16**, 6960 (2022).
 - [4] X. Jiang, Q. Liu, J. Xing, N. Liu, Y. Guo, Z. Liu, and J. Zhao, Recent progress on 2D magnets: Fundamental mechanism, structural design and modification, *Applied Physics Reviews* **8**, 031305 (2021).
 - [5] S. Chaudhuri, C. Kuo, Y. Chen, C. Lue, and J. Lin, Low-temperature magnetic order rearrangement in the layered van der Waals compound MnPS₃, *Physical Review B* **106**, 094416 (2022).
 - [6] D. Lançon, H. Walker, E. Ressouche, B. Ouladdiaf, K. Rule, G. McIntyre, T. Hicks, H. M. Rønnow, and A. Wildes, Magnetic structure and magnon dynamics of the quasi-two-dimensional antiferromagnet FePS₃, *Physical Review B* **94**, 214407 (2016).
 - [7] S. Liu, A. G. Del Águila, D. Bhowmick, C. K. Gan, T. T. H. Do, M. Prosnikov, D. Sedmidubský, Z. Sofer,

- P. C. Christianen, P. Sengupta, *et al.*, Direct observation of magnon-phonon strong coupling in two-dimensional antiferromagnet at high magnetic fields, *Physical Review Letters* **127**, 097401 (2021).
- [8] D. Vaclavkova, M. Palit, J. Wyzula, S. Ghosh, A. Delhomme, S. Maity, P. Kapuscinski, A. Ghosh, M. Veis, M. Grzeszczyk, *et al.*, Magnon polarons in the van der Waals antiferromagnet FePS₃, *Physical Review B* **104**, 134437 (2021).
- [9] A. Pawbake, T. Pelini, A. Delhomme, D. Romanin, D. Vaclavkova, G. Martinez, M. Calandra, M.-A. Measson, M. Veis, M. Potemski, *et al.*, High-pressure tuning of magnon-polarons in the layered antiferromagnet FePS₃, *ACS nano* **16**, 12656 (2022).
- [10] F. Dirnberger, R. Bushati, B. Datta, A. Kumar, A. H. MacDonald, E. Baldini, and V. M. Menon, Spin-correlated exciton-polaritons in a van der Waals magnet, *Nature Nanotechnology* **17**, 1060 (2022).
- [11] S. Kang, K. Kim, B. H. Kim, J. Kim, K. I. Sim, J.-U. Lee, S. Lee, K. Park, S. Yun, T. Kim, *et al.*, Coherent many-body exciton in van der Waals antiferromagnet NiPS₃, *Nature* **583**, 785 (2020).
- [12] A. R. Wildes, J. R. Stewart, M. D. Le, R. A. Ewings, K. C. Rule, G. Deng, and K. Anand, Magnetic dynamics of NiPS₃, *Phys. Rev. B* **106**, 174422 (2022).
- [13] C. Kim, J. Jeong, P. Park, T. Masuda, S. Asai, S. Itoh, H.-S. Kim, A. Wildes, and J.-G. Park, Spin waves in the two-dimensional honeycomb lattice xxz-type van der Waals antiferromagnet CoPS₃, *Physical Review B* **102**, 184429 (2020).
- [14] A. R. Wildes, B. Fåk, U. B. Hansen, M. Enderle, J. R. Stewart, L. Testa, H. M. Rønnow, C. Kim, and J.-G. Park, Spin wave spectra of single crystal CoPS₃, *Phys. Rev. B* **107**, 054438 (2023).
- [15] A. R. Wildes, V. Simonet, E. Ressouche, G. J. McIntyre, M. Avdeev, E. Suard, S. A. Kimber, D. Lançon, G. Pepe, B. Moubaraki, *et al.*, Magnetic structure of the quasi-two-dimensional antiferromagnet NiPS₃, *Physical Review B* **92**, 224408 (2015).
- [16] S. M. Rezende, A. Azevedo, and R. L. Rodríguez-Suárez, Introduction to antiferromagnetic magnons, *Journal of Applied Physics* **126**, 151101 (2019).
- [17] T. Y. Kim and C.-H. Park, Magnetic anisotropy and magnetic ordering of transition-metal phosphorus trisulfides, *Nano Letters* **21**, 10114 (2021).
- [18] M. Kobets, K. Dergachev, S. Gnatchenko, E. Khats'ko, Y. M. Vysochanskii, and M. Gurzan, Antiferromagnetic resonance in Mn₂P₂S₆, *Low Temperature Physics* **35**, 930 (2009).
- [19] D. Lançon, R. Ewings, T. Guidi, F. Formisano, and A. Wildes, Magnetic exchange parameters and anisotropy of the quasi-two-dimensional antiferromagnet NiPS₃, *Physical Review B* **98**, 134414 (2018).
- [20] T. T. Mai, K. F. Garrity, A. McCreary, J. Argo, J. R. Simpson, V. Doan-Nguyen, R. V. Aguilar, and A. R. H. Walker, Magnon-phonon hybridization in 2D antiferromagnet MnPSe₃, *Science advances* **7**, eabj3106 (2021).
- [21] D. Afanasiev, J. R. Hortensius, M. Matthiesen, S. Mañas-Valero, M. Šiškins, M. Lee, E. Lesne, H. S. van Der Zant, P. G. Steeneken, B. A. Ivanov, *et al.*, Controlling the anisotropy of a van der Waals antiferromagnet with light, *Science advances* **7**, 1 (2021).
- [22] C. A. Belvin, E. Baldini, I. O. Ozel, D. Mao, H. C. Po, C. J. Allington, S. Son, B. H. Kim, J. Kim, I. Hwang, *et al.*, Exciton-driven antiferromagnetic metal in a correlated van der Waals insulator, *Nature communications* **12**, 1 (2021).
- [23] K. Mehlawat, A. Alfonso, S. Selter, Y. Shemerliuk, S. Aswartham, B. Büchner, and V. Kataev, Low-energy excitations and magnetic anisotropy of the layered van der Waals antiferromagnet NiPS₃, *Physical Review B* **105**, 214427 (2022).
- [24] S. Y. Kim, T. Y. Kim, L. J. Sandilands, S. Sinn, M.-C. Lee, J. Son, S. Lee, K.-Y. Choi, W. Kim, B.-G. Park, *et al.*, Charge-spin correlation in van der Waals antiferromagnet NiPS₃, *Physical review letters* **120**, 136402 (2018).
- [25] X. Wang, J. Cao, Z. Lu, A. Cohen, H. Kitadai, T. Li, Q. Tan, M. Wilson, C. H. Lui, D. Smirnov, *et al.*, Spin-induced linear polarization of photoluminescence in antiferromagnetic van der Waals crystals, *Nature Materials* **20**, 964 (2021).
- [26] R. Basnet, A. Wegner, K. Pandey, S. Storment, and J. Hu, Highly sensitive spin-flop transition in antiferromagnetic van der Waals material MPS₃ (M = Ni, Mn), *Physical Review Materials* **5**, 064413 (2021).
- [27] R. Basnet, K. M. Kotur, M. Rybak, C. Stephenson, S. Bishop, C. Autieri, M. Birowska, and J. Hu, Controlling magnetic exchange and anisotropy by nonmagnetic ligand substitution in layered MPX₃ (M = Ni, Mn; X = S, Se), *Phys. Rev. Research* **4**, 023256 (2022).
- [28] F. Bougamha, S. Selter, Y. Shemerliuk, S. Aswartham, A. Benali, B. Büchner, H.-J. Grafe, and A. Dioguardi, P 31 NMR investigation of quasi-two-dimensional magnetic correlations in T₂P₂S₆ (T = Ni, Mn), *Physical Review B* **105**, 024410 (2022).
- [29] See Supplemental Material at [URL will be inserted by publisher] for details on sample preparation, experimental setup, phonon modes in NiPS₃, simulation for magnetic field dependence of Magnon branches, and rotation of X-transition PL polarization.
- [30] K. Momma and F. Izumi, Vesta 3 for three-dimensional visualization of crystal, volumetric and morphology data, *Journal of applied crystallography* **44**, 1272 (2011).
- [31] T. Nagamiya, K. Yosida, and R. Kubo, Antiferromagnetism, *Advances in Physics* **4**, 1 (1955).
- [32] P. Joy and S. Vasudevan, Magnetism in the layered transition-metal thiophosphates MPS₃ (M = Mn, Fe and Ni), *Physical Review B* **46**, 5425 (1992).
- [33] S. Gnatchenko, I. Kachur, V. Piryatinskaya, Y. M. Vysochanskii, and M. Gurzan, Exciton-magnon structure of the optical absorption spectrum of antiferromagnetic MnPS₃, *Low Temperature Physics* **37**, 144 (2011).

Supplemental Material for "Magnon excitations and spin-entangled excitons in van der Waals antiferromagnet NiPS₃"

Dipankar Jana,^{1,*} P. Kapuscinski,¹ I. Mohelsky,¹ D. Vaclavkova,¹
I. Breslavetz,¹ M. Orlita,^{1,2} C. Faugeras,¹ and M. Potemski^{1,3,†}

¹*Laboratoire National des Champs Magnétiques Intenses, LNCMI-EMFL,
CNRS UPR3228, Univ. Grenoble Alpes, Univ. Toulouse,
Univ. Toulouse 3, INSA-T, Grenoble and Toulouse, France*

²*Institute of Physics, Charles University, Ke Karlovu 5, Prague, 121 16, Czech Republic*

³*CENTERA Labs, Institute of High Pressure Physics, PAS, 01 - 142 Warsaw, Poland*

I. EXPERIMENTAL DETAILS

A. Sample preparation

As already mentioned in the main text, the samples used in our experiments were extracted from commercially available bulk NiPS₃ crystals. The crystals we have used were not however perfectly homogeneous but composed of "twisted" grains, with different crystal axis orientations in the layers', a-b plane. The isolation of single crystals (with well defined, a,b crystallographic axes in their entire volume), has been a critical point for the majority of the experiments presented in our work. These experiments (micro-Raman and micro-photoluminescence measurements versus in-plane magnetic field B) has been carried out on relatively small size flakes exfoliated from bulk NiPS₃ crystals and transferred on silicon substrates. Each flake has been primarily characterized by polarization resolved photoluminescence (PL) measurements (at low temperature and $B = 0$) of the X-transition (see the main text). The X-transition is linearly polarized because it is coupled to spins which are aligned along the a-crystal axis [S1]. In the ideal case of perfectly uniform NiPS₃ crystals, the polarization degree of the X-emission is expected to reach the unity. The compromise criterion to select samples for further experiments was to choose those which display the polarization degree larger than 0.8. The issue of the crystal homogeneity was not however essential for the experiments carried out as a function of the magnetic field applied perpendicularly to the layer planes. In such a geometry, the direction of the spin alignment is always perpendicular to the applied magnetic field, independent on the crystallites' orientation in the a,b plane. Thus, using large samples unavoidable for far-infrared transmission measurements was justified in experiments with Faraday-geometry.

B. Experimental set-up

Micro-optical arrangement has been applied in all Raman scattering and photoluminescence measurements presented in our work. The continuous-wave laser operational at 515 nm was used as the excitation source. The laser beam has been focused via 50 X microscope objectives providing $\sim 2 \mu\text{m}$ in diameters spot on the samples. The emitted/scattered light, collected via the same objective, was dispersed with a 0.7 m long monochromator and detected with a nitrogen-cooled charge coupled device camera. Experiments as a function of temperature are carried out by placing sample on the cold finger of a continuous flow cryostat which is mounted on x-y positioners. In case of measurements conducted as a function of the magnetic field we used a free-beam insert placed in a superconducting magnet supplying the magnetic fields up to 14 T. The x-y-z piezo stage with the sample placed on it and microscope objective fixed above have been altogether immersed in a tube filled in with gaseous helium, in contacts with bath of liquid helium.

When measuring the Raman scattering signals, special efforts have been made to efficiently reject the stray laser light. First of all, both the excitation beam and the out-coming light were passed through the sets of triple Bragg filters. To further suppress the stray laser light a certain angle was set between the direction of the incident laser beam and the direction normal to the surface sample (crystal c-axis). This angle was fixed at 20° in case of field dependent experiments, the results of which are presented in Fig. 3, Fig. 5 and Fig. 8 of main text. It was fixed at 30° in the experiments carried out as a function of temperature (see Fig. 2 of the main text and Fig. S1). It should be,

* dipankar.jana@lncmi.cnrs.fr

† marek.potemski@lncmi.cnrs.fr

however, noted that the direction of the excitation beam was kept parallel to the c-axis in case of photoluminescence measurements illustrated in Fig. 7 of the main text.

Far-infrared magneto-transmission experiments were carried out on large area NiPS₃ specimens which were kept in helium exchange gas at temperature of 4.2 K and placed in a superconducting solenoid magnet. The magnetic field was always applied perpendicular to the quasi-two-dimensional plane and aligned with the wave vector of the probing radiation (Faraday configuration). To measure the magneto-transmission, the radiation from a mercury lamp was modulated by a Bruker Vertex 80v Fourier-transform spectrometer, delivered to the sample via light-pipe optics and then detected by a composite bolometer placed directly behind the sample.

II. RAMAN SCATTERING RESPONSE OF NiPS₃ IN A WIDE SPECTRAL RANGE: MAGNON AND PHONON EXCITATIONS

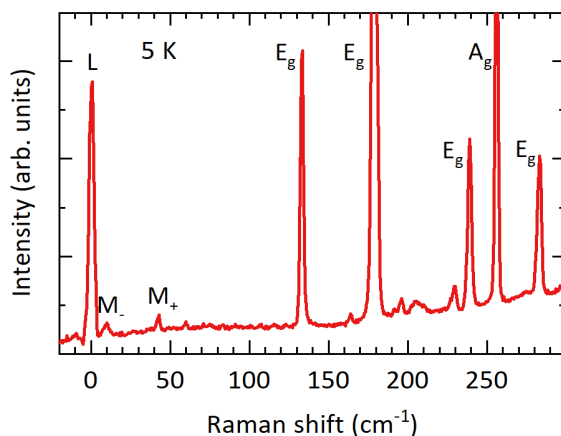


FIG. S1. Low temperature (10 K) Raman scattering spectrum of NiPS₃ in a broad energy range. M_- and M_+ peaks are due to magnon gap excitations extensively characterized in the main text, whereas E_g and A_g denote the symmetries of the characteristic phonon excitations identified in previous studies [S2–S4].

Our Raman scattering study presented in the main text, has been focused on the low energy excitations which appear in the close vicinity of the laser line. We have, however, also measured the Raman scattering spectra in a wide spectral range. An example of such a spectrum is illustrated in Fig. S1. The features seen in this spectrum at energies above 50 cm^{-1} are due to characteristic phonon excitations in NiPS₃, that has been previously reported and characterized [S2–S4]. We note that Raman peaks due to phonon excitations are significantly more intense than those associated to M_+ and M_- magnon gap excitations which are the central point of the present work.

III. NUMERICAL SIMULATIONS FOR THE IN-PLANE MAGNETIC FIELD DEPENDENT SPIN ROTATION AND MAGNON GAP ENERGIES

As discussed in the main part of the text, the evolution, upon the application of the in-plane magnetic field, of magnon gaps and the associated rotation of the spin ensemble in NiPS₃ antiferromagnet can be described with the solutions of Eq. 1 and Eq. 3 of the main text. Critical parameter in these solutions is the angle θ_B between the direction of the applied field and the magnetic moment alignment (i.e. the crystal a-axis) in the absence of the magnetic field. A pictorial illustration of the rotation of the spin assembly in NiPS₃ upon application of the in-plane magnetic field aligned at certain $\theta_B \neq 0$ angle is presented in Fig. S2. When increasing the magnetic field, the spins rotate towards the direction perpendicular to the magnetic field, the rotation being quantified by the angle Ψ between the field direction and the apparent axis of the spin alignment. At sufficiently high fields, above the spin flop field, the spins are aligned nearly perpendicular to the magnetic field ($\Psi \sim 90^\circ$). Obviously, upon further increase of the magnetic field the antiferromagnetic spin order should progressively turn into the ferromagnetic one with all spins aligned along the field direction. The numerical solution of the Eq. 1 and Eq. 3, for the B-dependence of Ψ , w_{M_-} and w_{M_+} are presented in Fig. S3 for several selected angle θ_B . All traces in these figures have been plotted

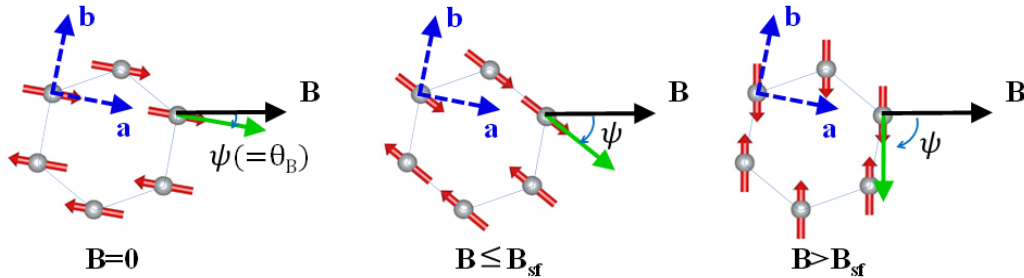


FIG. S2. A pictorial illustration of the rotation of the spin assembly in NiPS_3 upon application of the in-plane magnetic field.

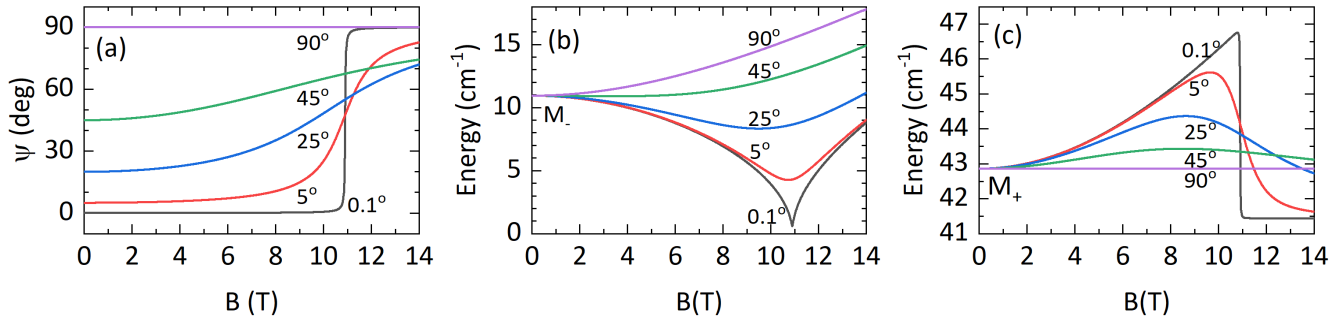


FIG. S3. (a) Simulated in-plane magnetic field dependence of Ψ for different values of θ_B , (b) and (c) Simulated in-plane magnetic field dependence of low M_- and high M_+ energy magnon modes respectively for different θ_B .

assuming a common set of other parameters: $g = 2.15$, $w_{M_-} = 11 \text{ cm}^{-1}$ and $w_{M_+} = 42.7 \text{ cm}^{-1}$ respectively, for the g -factor and two magnon gap energies at $B = 0\text{T}$ (see the main text). The results of calculations shown in Fig.S3 are in support to the analysis of the experimental data presented in Fig. 4 of the main text. To this end it is worth noting that analytical solutions can be obtained in the limit of $\theta_B = 0^\circ$. As already presented in the main text, $w_{M_+} = g\mu_B\sqrt{C_2 + 3B^2}$ and $w_{M_-} = g\mu_B\sqrt{C_1 - B^2}$ for $B \leq B_{sf}$. When $B \geq B_{sf}$, the field dependence of magnon mode energies are given by [S5] $w_{M_-} = g\mu_B\sqrt{B^2 - C_1}$ and $w_{M_+} = g\mu_B\sqrt{C_2 - C_1}$. Spins remain aligned along the a -axis until the spin-flop field at which they rotate abruptly to align perpendicularly to the magnetic field (along the b -crystal axis).

IV. IN-PLANE MAGNETIC FIELD DEPENDENT ROTATION OF X-TRANSITION PL POLARIZATION

As mentioned before, the X-transition is expected to be linearly polarized due to coupling with spin alignment. The rotation of the Ni^{2+} spins' alignment induced by the application of the in-plane magnetic field (see Fig. S3 (a)) will therefore impose the rotation of the axis of linear polarization of X-transition. This effect is illustrated in Fig. S4, for the case when the applied magnetic field is nearly parallel ($\theta_B = 5^\circ$) to the initial (at $B = 0\text{ T}$) alignment of Ni^{2+} spins (the data are complementary to those presented in Fig. 7 of the main text). A high degree of linear polarization confirms unidirectional spin orientation of the investigated flake while the significant turn of the PL polarization axis after the spin-flop field establishes the field-induced spin rotation.

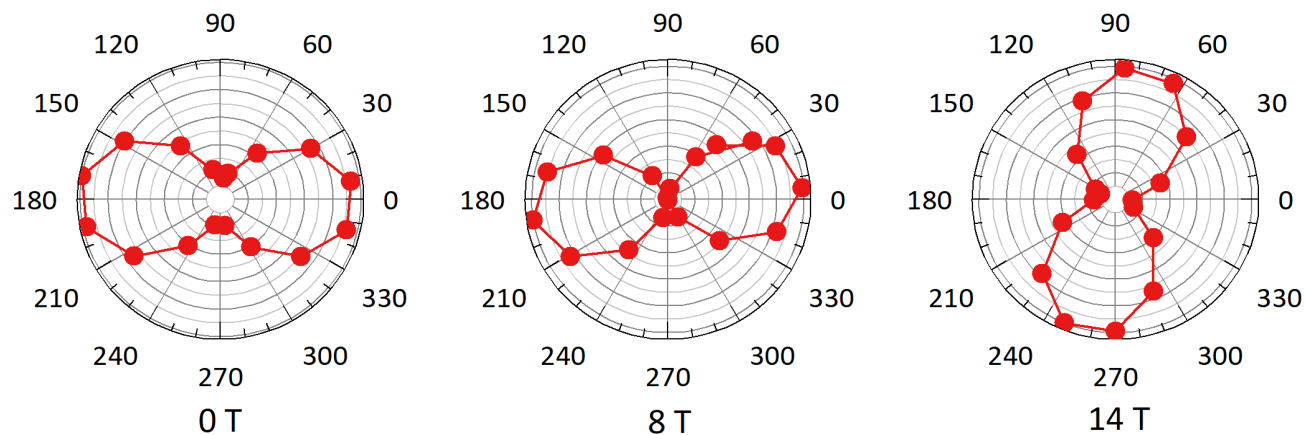


FIG. S4. Polar plots of linear polarization resolved integrated photoluminescence intensity of the upper component of the X_+ -transition at different magnetic fields applied in the in-plane direction (the corresponding traces for the X_- -component are identical). The presented data complete those presented in Fig. 7 of the main text. Both data sets have been obtained for the same NiPS_3 flake, and the geometry of the applied field was also the same. A contribution of Faraday rotation induced by the objective lens has been subtracted and the polarization orientation at $B = 0$ T was taken as a reference and set as 0° axis.

-
- [S1] Q. H. Wang, A. Bedoya-Pinto, M. Blei, A. H. Dismukes, A. Hamo, S. Jenkins, M. Koperski, Y. Liu, Q.-C. Sun, E. J. Telford, *et al.*, The magnetic genome of two-dimensional van der waals materials, *ACS nano* **16**, 6960 (2022).
- [S2] X. Wang, J. Cao, Z. Lu, A. Cohen, H. Kitadai, T. Li, Q. Tan, M. Wilson, C. H. Lui, D. Smirnov, *et al.*, Spin-induced linear polarization of photoluminescence in antiferromagnetic van der waals crystals, *Nature Materials* **20**, 964 (2021).
- [S3] S. Y. Kim, T. Y. Kim, L. J. Sandilands, S. Sinn, M.-C. Lee, J. Son, S. Lee, K.-Y. Choi, W. Kim, B.-G. Park, *et al.*, Charge-spin correlation in van der waals antiferromagnet NiPS_3 , *Physical review letters* **120**, 136402 (2018).
- [S4] C. Kim, J. Jeong, P. Park, T. Masuda, S. Asai, S. Itoh, H.-S. Kim, A. Wildes, and J.-G. Park, Spin waves in the two-dimensional honeycomb lattice xxz-type van der waals antiferromagnet NiPS_3 , *Physical Review B* **102**, 184429 (2020).
- [S5] S. M. Rezende, A. Azevedo, and R. L. Rodríguez-Suárez, Introduction to antiferromagnetic magnons, *Journal of Applied Physics* **126**, 151101 (2019).